



Low Frequency Noise Attenuation inside Ducts using locally resonant periodic flush mounted Steel Patches

Maaz Farooqui, Tamer Elnady and Wael Akl

ASU Sound and Vibration Lab, Faculty of Engineering, Ain Shams University, Cairo, Egypt

Summary

Traditional passive noise control techniques using Helmholtz resonators have size limitations at low frequency due to the long wavelengths. Promising noise reductions, with flush mounted Stainless Steel patches with no such constraints can be obtained building on local resonance phenomenon implemented in acoustic metamaterials techniques. The objective of the current paper is to introduce locally resonant thin Steel patches flush mounted to an acoustic duct walls aiming at creating frequency stop bands at the low frequency zone (below 1 KHz). Green's Function is used under the framework of interface response theory to predict the degree of attenuation of the local resonant patches. The experimental results were compared with Analytical theory and Finite elements and a close agreement was found.

PACS no 43.35.Gk, 43.50.Gf

1. Introduction

In the last couple of decades, phononic crystals have received increased attention both theoretically [1]–[4] and experimentally [5]–[9]. Small dimensional structures which have a regular distribution of scattering centers have been seen to possess a distinct and interesting array of acoustical properties, perhaps most strikingly frequency band gaps within which acoustic waves cannot propagate through the structure—a so-called phononic band gap within which propagation of sound, vibration, and phonons are all forbidden. The position and the width of the band gap are critical parameters for devices that reflect or localize the acoustic waves [4]. These acoustic band gap materials can have many practical applications such as elastic/acoustic filters, acoustic wave-guides, sonic lens, cavities, acoustic isolators and sensors. [10]–[13]

In a perfect resonance phononic crystal, the band gaps are introduced by two mechanisms. One is due to the local resonance with the resonator when a frequency of the sound wave coincides with its Eigen mode frequency. [14] The other is due to the

Bragg reflection when the periodic spacing between the neighboring resonators becomes a multiple of a half-wavelength of the sound wave. Band gaps are the result of wave scattering at periodic impedance mismatch zones (Bragg scattering) or are generated by resonating units within the medium. While Bragg scattering band gaps occur at wavelengths of the order of the unit cell size, local resonances produce frequency attenuation regions which are independent of the lattice constant defining the spatial periodicity of the medium. For this reason, locally resonant materials are of particular interest due to their ability to generate low frequency attenuation and the possibility of providing the medium with unusual mechanical properties at long wavelengths. The latter is the main objective in the study and development of acoustic metamaterials. Replacing the classical Helmholtz resonators we propose frequency tailored patches for noise reduction in ducts.

Locally resonating acoustic metamaterials have been implemented by considering single and multiple degrees of freedom resonating units such as soft inclusions periodically dispersed in a hard material matrix [3], [15] or periodic arrays of tuned Helmholtz resonators in an acoustic waveguide [14], [16]. Bragg-scattering-induced

band gaps in phononic crystals exist when their mass density and bulk modulus are spatially modulated [11], [17].

The objective of the current paper is to introduce locally resonant Steel patches flush mounted to an acoustic duct walls aiming at creating frequency stop bands at the low frequency zone. Inverse surface Green's Function is used to predict the performance of the local resonant patches. Realistic techniques for expanding the stop bandwidth have been introduced and the mutual effect of the locally resonant patches in conjunction with the Bragg band gap has been investigated. Our study is performed using the interface response theory of continuous media [18]. The plan of this work is as follows: The inverse surface Green's function of the suggested system containing the patches and waveguide tube is derived. Mechanisms for broadening the band gap, by adding damping and lumped masses are presented in the analytical model. The analytical model is then validated using COMSOL Multiphysics.

2. Green's function formulation

The wave propagation in a homogeneous solid can be strongly altered by inserting periodical inclusions with different elastic constants. The periodic inclusions in these so-called Phononic Crystals (PCs) induce a wave scattering and destructive interferences that appear in some frequency ranges, leading to forbidden band-gaps. Total reflection is then expected in these frequency ranges. The inverse surface Green's function of a semi-infinite waveguide tube is given as formerly introduced in [4], [14], [19]

$$[g_s]^{-1} = -j/Z \quad (1)$$

with $Z = \rho c/a$ being the acoustic impedance of a tube-shaped material, ρ , c being the density and the sound speed of the material, respectively, and 'a' being the cross-sectional area of the waveguide.

The inverse surface Green's function of a finite slab shown in Figure 1 with a length L and admittance F and angular frequency ω under the closed boundary condition [19] can be simplified and written in the form

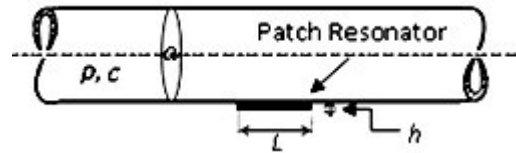


Figure 1. Schematic of the geometry of a waveguide tube. a is the cross-sectional area of the waveguide tube. The local resonator is patch with a length L and a height h .

$$[G_i]^{-1} = (j/Z_i \sin(\omega L_i/c)) \begin{bmatrix} \cos(\omega L_i/c) & 1 \\ 1 & \cos(\omega L_i/c) \end{bmatrix} \quad (2)$$

where Z_i , the impedance of a thin plate with a high aspect ration clamped at the boundaries having a density ρ_1 , Young's Modulus Y_0 , Poisson ratio ν , width L and height h can be written as [20]

$$Z_i = \left(\frac{k_1 k_2 L h \rho_1 \omega}{k_1 k_2 L - 2 c_2 k_1 h \rho_1 \omega^2 \sin \frac{k_2 L}{2} - 4 c_1 k_2 h \rho_1 \omega^2 \sinh \frac{k_1 L}{2}} \right) \quad (3)$$

where,

$$c_1 = \frac{k_2 \sin \frac{L k_2}{2}}{h \rho_1 \omega^2 (2 k_1 \sinh \frac{L k_1}{2} \cos \frac{L k_2}{2} + 2 k_2 \sin \frac{L k_2}{2} \cosh \frac{L k_1}{2})} \quad (4)$$

$$c_2 = \frac{k_1 \sinh \frac{L k_1}{2}}{h \rho_1 \omega^2 (k_1 \sinh \frac{L k_1}{2} \cos \frac{L k_2}{2} + k_2 \sin \frac{L k_2}{2} \cosh \frac{L k_1}{2})} \quad (5)$$

$$c = \frac{(Y_0) h^2}{12 \rho_1 (1 - \nu^2)} \quad \text{and} \quad k_1 = k_2 = \sqrt{\frac{\omega}{\sqrt{c}}}$$

The inverse Green's function for the patch in contact with the waveguide tube becomes

$$g_p^{-1} = \frac{j \cos(\omega L_p/c)}{Z_p \sin(\omega L_p/c)} \quad (6)$$

where Z_p , L_p is the impedance and length of the patch respectively. Similarly, the impedance for a circular patch [21] can also be derived and used instead of that of rectangular patches.

The interface domain of the composite system of Figure 2 is reduced to one point, and thus, the inverse interface Green's function of the whole system can be obtained as the sum of the inverse Green's functions of the two semi-infinite tubes and the patch[5], [14], [16]

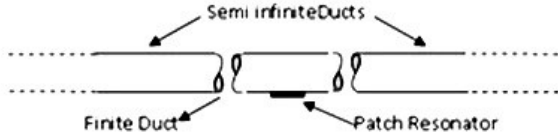


Figure 2. Schematic of the final geometry of the system, a finite sized duct with the patch with semi-infinite wave guide tubes on both sides.

$$G^{-1} = \frac{-2i}{Z_1} + g_p^{-1} \quad (7)$$

where Z_1 is the impedance of the slender tube. And the transmission coefficient, t , for one patch can be calculated by the relation [14], [16]

$$t = (2i / Z_1) \cdot G \quad (8)$$

A composite system is constructed cut out of the infinite periodic system. This finite structure is connected at its ends to two semi-infinite leading tubes. The finite structure is therefore composed of N patches grafted periodically with a spacing d_1 on a finite slender tube. For this new system, the inverse interface Green's function is a finite banded matrix defined in the interface domain of all the connection points [14]

$$G_N^{-1} = \begin{bmatrix} A' & B & 0 & \dots & 0 & 0 & 0 \\ B & A & B & \dots & 0 & 0 & 0 \\ 0 & B & 0 & \dots & 0 & 0 & 0 \\ \vdots & \vdots & \vdots & \ddots & \vdots & \vdots & \vdots \\ 0 & 0 & 0 & \dots & A & B & 0 \\ 0 & 0 & 0 & \dots & B & A & B \\ 0 & 0 & 0 & \dots & 0 & B & A'' \end{bmatrix} \quad (9)$$

The values of elements of this matrix G_N^{-1} can be obtained from reference [14]. The transmission factor can be formulated as [14],[16]

$$T = \left| \frac{2 \cdot \text{Sin}(\alpha_1 \cdot d_1) \cdot (e^{i \cdot N \cdot k \cdot d_1} - 1) \cdot e^{i \cdot N \cdot k \cdot d_1}}{(1 - e^{i \cdot (\alpha_1 + k) \cdot d_1})^2 - e^{i \cdot 2 \cdot N \cdot k \cdot d_1} (e^{i \cdot k \cdot d_1} - e^{i \cdot \alpha_1 \cdot d_1})^2} \right|^2 \quad (10)$$

Here N is the number of patches, and k represents the Bragg wave vector of the infinite system and $\alpha_1 = j\omega/c$. Similarly, the reflection coefficient can be expressed in the form [16]

$$R = \left| \frac{2i}{Z_p} G(1,1) - 1 \right|^2 \quad (11)$$

2.1 Broadening of the stop bandwidth

Viscous damping has been introduced to the proposed system by adding viscous damping layers on the patches in the experiments. Lumped masses of steel have also been added to the patches to further broaden the band gaps. The Rayleigh damping is the most common way to describe the damping present in the patches. Where α is the mass multiplication factor and β is the stiffness multiplication factor. For Rayleigh damping $\alpha \geq 0$ and $\beta \geq 0$. [25],[26]

The values of α and β are dependent on energy dissipation characteristic of structure and determined through modal damping ratios. The damping coefficient can be calculated using the formula [25],[27]

$$\xi = \frac{\alpha}{2\omega_i} + \frac{\omega_i\beta}{2} \quad (12)$$

Where ω_i corresponds to the different resonant frequencies of the system. This has been incorporated in the analytical model by a change in the impedance of patches which is governed by equation 3. The respective impedance of the lumped masses was added in series with the impedance of patches and the equivalent impedance represented the net impedance of the new mass-patch system.

3. Experimental Setup

A test rig was developed and two source technique was used to measure the attenuation achieved from a single patch as in Figure 3. The test rig consists of wooden duct 4000 mm in length and with 70 mm square cross section and has a wall thickness of 22 mm. Six ¼ inch B&K 4944A microphones flush mounted in the duct wall, three upstream and three downstream of the test object, were used to cover the plane wave range in the test duct. Signals from the loudspeaker and from the microphones are fed into a PXI Controller data acquisition system as input signals and output signals. The signal from the loudspeaker is used as the reference signal. Both input and output signals are converted into digital signals by the NI acquisition system and then processed by SIDLAB acquisition (A LabView Program used to determine the Transmission Loss by the wave decomposition method).

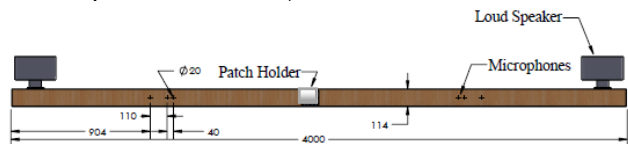


Figure 3. Realization of the test rig used for the measurements of the Transmission characteristics of the patch (All dimensions in mm).

4. Results and Discussions

COMSOL, a FEM based software was used for modeling the system of patches numerically. A 3D model containing one Steel patch (53 x 35 x 0.15) mm³ in the center of the duct was simulated first and the transmission coefficient of this patch

was calculated. The resonance frequency if these patches were around 810 Hz. The surface SPL response of the duct is shown in Figure 4. The three views depicted in this figure illustrate the attenuation mechanism followed by the wave under the effect of the locally resonant Stainless Steel AISI 430 patch with chemical composition (Fe: 81/Cr: 17/Mn / Si/ C/ S/ P). Since only plane wave range is assumed in this study, the formation of plane wave and its reflection as soon as it reaches the specimen can be easily visualized in figure 4. The attenuation observed numerically in this very case was around 25 decibels.

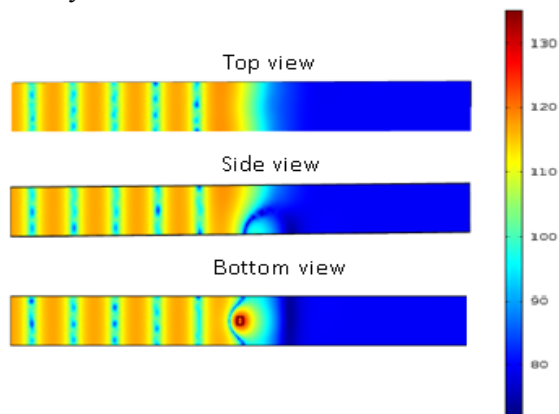


Figure 4. SPL response (dB) of the 3D Steel patch clamped at the boundaries

The outdoor radiation from the patch was controlled by sound hard boundary wall condition in the COMSOL simulations which doesn't allow any sound to escape from the patch.

We tried to model Aluminum patches at the first instance using Green's function and Finite element method (COMSOL). The sound attenuation offered by these patches was sufficiently high but in the measurements we discovered that the patches buckled after few days of measurements with or without flow. The buckling load for Aluminum was considerably low and due to this a shift in the resonant frequency of the patches was observed after few days of measurements. We needed a material similar to Aluminum but with a higher buckling load i.e. higher Young's Modulus. Steel was the best option available for us, which was not only ubiquitous but also robust and cheaper alternative to Aluminum.

The Transmission coefficients were modeled for a number of different Aluminum patch ($53 \times 35 \times 0.1$) mm³ configurations inside the duct using COMSOL. The resonance frequency of these patches was around 550 Hz. There were two important boundary conditions assumed in these

simulations. The patch is fixed from all the four sides and, only plane wave propagates at the ends of the duct. The fluid medium used in all simulations is air. The effect of three different levels of Rayleigh damping applied on the patch can be visualized in Figure 5, where the change in the levels of damping served the purpose of broadening the area under the transmission curve. Though, it is a trade-off with the quality of attenuation, it also serves in the smoothing of the curve when a number of peaks are juxtaposed on it. The surface SPL response of the ten patches simulation is shown in Figure 6. Some small peaks are observed around the curve for ($\text{Alpha}=0$, $\text{Beta}=0$), which is attributed to Bragg's scattering happening due to the array of patches with a lattice constant of 15 cm. Similar effects can be seen in Figure 7 due to the same reason.

As discussed earlier, the main objective of the study was to investigate the local resonance attenuation. Hence, increasing the number of patches was to investigate the effect of the number of patches (local resonators) on the noise attenuation rather than to introduce Bragg scattering effect. For the sake of clarity all the simulations were done at gaps which were not multiples of halves of the wave length of the excitation.

In order to save computational time Green's function analytical model was implemented first. Three different configurations of Aluminum patches were considered in this case. One patch, ten patches without damping and lumped masses, and ten patches with damping and lumped masses. The comparison of the transmission coefficients achieved in the three cases is shown in Figure 7.

A simple case of one steel patch flush mounted to the duct (Figure 3) was measured and the patch exhibited similar resonance characteristic in the expected range of frequency. Figure 8 depicts the comparison of measurement with Numerical and Analytical results. As discussed earlier the occurrence of non-unity transmission coefficient resembles duct vibrations due to its shape and some absorption of sound because of the material of the duct which was wood in this case.

We varnished the duct from inside to reduce this kind of sound absorption but still some acoustic leakage and duct vibrations led to non-unity transmission coefficient at some frequencies.

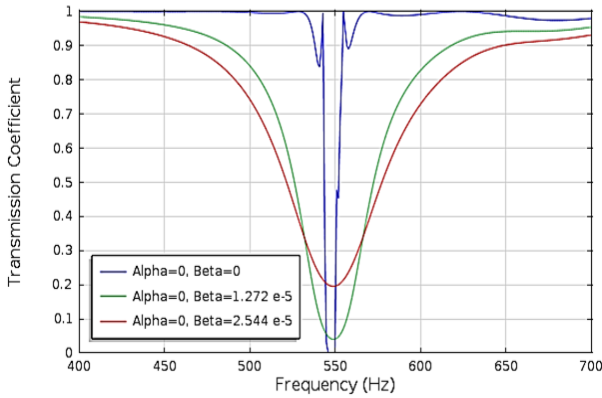


Figure 5. Numerically calculated Transmission Coefficient for the duct with three different configurations of dampings applied to ten Aluminum patches.

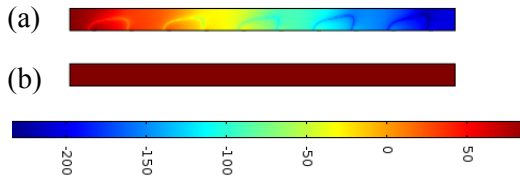


Figure 6. Sound pressure level (dB) in a duct (a) with the Aluminum patches (b) Without any resonators.

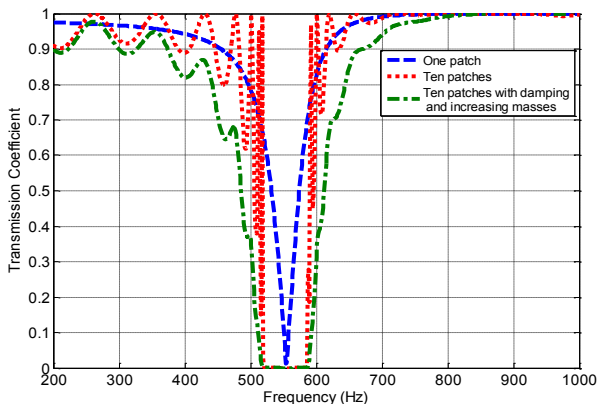


Figure 7. Analytical results for three different configurations of Aluminum patches.

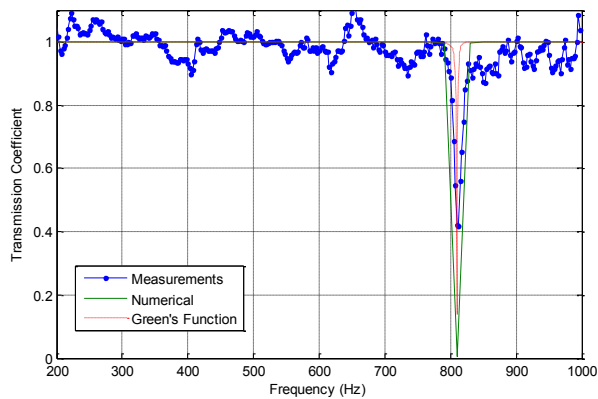


Figure 8. Transmission coefficients for one steel patch from modelling techniques and measurements.

In order to stop any sound radiation out of the duct through the patch, we covered the patch with an enclosure specially designed for the patches as in Figure 9. This wooden enclosure consisted of porous absorbers, to absorb any noise that is ejected out of the duct through the patch. On measuring this system with the enclosure we discovered that the resonance frequency of the steel patch was not at all affected by the enclosure (Figure 10).

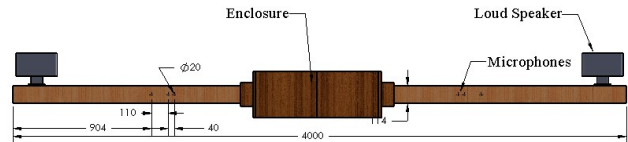


Figure 9. Realization of the test rig used with enclosure (All dimensions in mm).

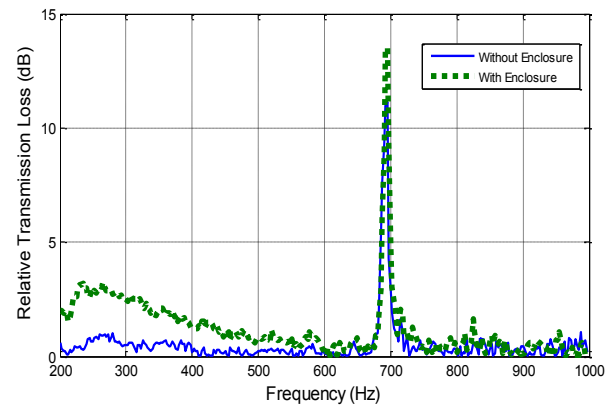


Figure 10. Relative transmission Loss (dB) for two cascaded steel patches with and without enclosure.

5. Conclusions

A systematic study of the propagation of the acoustic waves in phononic crystals containing locally resonant periodic flush mounted flexible Patches was carried out.

The band structure and the transmission spectrum were studied for different configurations without any restrictions using the interface response theory. Significant transmission loss, which gave rise to absolute band gaps in the acoustic band of a periodic structure, was obtained. In addition to the band gaps formed due to local resonance effect, other band gaps, due to Bragg's scattering, existed due to the periodic nature of the structure. In the configurations studied, the gap width is controlled by the geometrical parameters including the dimensions of the patches and the periodic gaps of the structure.

The analytical analysis of the stop bands of these Metamaterials were compared with the Numerical results obtained from COMSOL Multiphysics. The results show reasonable agreements with the theory. The accuracy of FEM based simulation was restricted by the computational capabilities available. The analytical model can hence be regarded as an alternative to the FEM with a reduced computational cost and improved accuracy.

Acknowledgments

This research was supported by the FP7 Marie Curie Initial Training Network (ITN) Silent Air Flows in transport, buildings, and power generation (FlowAirS), contract number 289352.

References

- [1] R. Zhu, G. L. Huang, and G. K. Hu, "Effective Dynamic Properties and Multi-Resonant Design of Acoustic Metamaterials," *J. Vib. Acoust.*, vol. 134, no. 3, p. 031006, 2012.
- [2] J. Yeh, "Wave propagation analysis and application of the phononic crystal with defect inserts," *J. Eng. Technol.*, vol. 6, no. 3, pp. 309–315, 2009.
- [3] H. Assi, "Acoustic Metamaterials: Theory and Potential Applications," no. 993444251, pp. 1–9, 1960.
- [4] E. H. El Boudouti, T. Mrabti, H. Al-Wahsh, B. Djafari-Rouhani, A. Akjouj, and L. Dobrzynski, "Transmission gaps and Fano resonances in an acoustic waveguide: analytical model," *J. Phys. Condens. Matter*, vol. 20, no. 25, p. 255212, Jun. 2008.
- [5] E. H. El Boudouti, "Experimental and theoretical evidence for the existence of photonic bandgaps and selective transmissions in serial loop structures," *J. Appl. Phys.*, vol. 95, no. 3, p. 1102, 2004.
- [6] W. N. Bulk-modulus, "Experimental And Theoretical Investigation Of Acoustic Metamaterial," 2011.
- [7] X. Wang and C. M. Mak, "Acoustic performance of a duct loaded with identical resonators.," *J. Acoust. Soc. Am.*, vol. 131, no. 4, pp. EL316–22, Apr. 2012.
- [8] B. Hou, J. Mei, M. Ke, Z. Liu, J. Shi, and W. Wen, "Experimental determination for resonance-induced transmission of acoustic waves through subwavelength hole arrays," *J. Appl. Phys.*, vol. 104, no. 1, p. 014909, 2008.
- [9] Z. Yang, H. M. Dai, N. H. Chan, G. C. Ma, and P. Sheng, "Acoustic metamaterial panels for sound attenuation in the 50–1000 Hz regime," *Appl. Phys. Lett.*, vol. 96, no. 4, p. 041906, 2010.
- [10] X.-F. Zhu, "Acoustic waves switch based on meta-fluid phononic crystals," *J. Appl. Phys.*, vol. 112, no. 4, p. 044509, 2012.
- [11] H. C. Zeng, C. R. Luo, H. J. Chen, S. L. Zhai, and X. P. Zhao, "Flute-Model Acoustic Metamaterials with Simultaneously Negative Bulk Modulus and Mass Density," pp. 1–11.
- [12] S.-C. S. Lin, B. R. Tittmann, and T. J. Huang, "Design of acoustic beam aperture modifier using gradient-index phononic crystals.," *J. Appl. Phys.*, vol. 111, no. 12, p. 123510, Jun. 2012.
- [13] F. Casadei, T. Delpero, A. Bergamini, P. Ermanni, and M. Ruzzene, "Piezoelectric resonator arrays for tunable acoustic waveguides and metamaterials," *J. Appl. Phys.*, vol. 112, no. 6, p. 064902, 2012.
- [14] Z. G. Wang, S. H. Lee, C. K. Kim, C. M. Park, K. Nahm, and S. A. Nikitov, "Acoustic wave propagation in one-dimensional phononic crystals containing Helmholtz resonators," *J. Appl. Phys.*, vol. 103, no. 6, p. 064907, 2008.
- [15] N. Swintek, J. O. Vasseur, a. C. Hladky-Hennion, C. Croëne, S. Bringuier, and P. a. Deymier, "Multifunctional solid/solid phononic crystal," *J. Appl. Phys.*, vol. 112, no. 2, p. 024514, 2012.
- [16] Z. G. Wang, S. H. Lee, C. K. Kim, C. M. Park, K. Nahm, and S. A. Nikitov, "Effective medium theory of the one-dimensional resonance phononic crystal," *J. Phys. Condens. Matter*, vol. 20, no. 5, p. 055209, Feb. 2008.
- [17] W. Akl and A. Baz, "Multi-cell Active Acoustic Metamaterial with Programmable Bulk Modulus", *Journal of Intelligent Material Systems and Structures* 2010; 21; 541
- [18] E. Elboudouti, "Acoustic waves in solid and fluid layered materials," *Surf. Sci. Rep.*, vol. 64, no. 11, pp. 471–594, Nov. 2009.
- [19] H. Al-Wahsh, a. Akjouj, B. Djafari-Rouhani, J. Vasseur, L. Dobrzynski, and P. Deymier, "Large magnonic band gaps and defect modes in one-dimensional comblike structures," *Phys. Rev. B*, vol. 59, no. 13, pp. 8709–8719, Apr. 1999.
- [20] M. H. Badi, S. Member, G. G. Yaralioglu, A. S. Ergun, S. T. Hansen, E. J. Wong, and B. T. Khuriyaku, "Capacitive Micromachined Ultrasonic Lamb Wave Transducers using Rectangular membranes," vol. 50, no. 9, pp. 1191–1203, 2003.
- [21] L. Seung-Mok, C. Bu-sang, and O. Masanori, "Viscous Damping Effect on the CMUT Device in Air," *J. Korean Phys. Soc.*, vol. 58, no. 4, p. 747, Apr. 2011.
- [22] D. R. Smith, S. Schultz, and C. M. Soukoulis, "Determination of Negative Permittivity and Permeability of Metamaterials from Reflection and Transmission Coefficients," pp. 1–5, 2002.
- [23] V. Fokin, M. Ambati, C. Sun, and X. Zhang, "Method for retrieving effective properties of locally resonant acoustic metamaterials," no. April, pp. 1–5, 2007.
- [25] R. E. Spears and S. R. Jensen, "Approach for Selection of Rayleigh Damping Parameters Used for Time History Analysis." Vol. 8 *Seism. Eng.* 17–24 (2009). doi:10.1115/PVP2009-77257
- [26] S. Adhikari and A. S. Phani, "Rayleigh's Classical Damping Revisited". 1–23 (2004).
- [27] S. Adhikari and J. Woodhouse, "Identification of Damping: Part 1, Viscous Damping." *J. Sound Vib.* 243, 43–61 (2001).